ROYAL SOCIETY
OF CHEMISTRY

PAPER

Check for updates

A rechargeable metal-free full-liquid sulfur–bromine battery for sustainable energy storage†

Lina Wang, [ID] *[a] Xiaofei Wang,[a] Jingyuan Liu,[b] Hao Yang,[a] Cuimei Fu,[a] Yongyao Xia [ID] *[b] and Tianxi Liu [ID] *[a]

The broad application of lithium–sulfur technology is far from viable unless the obstacles associated with the dissolution of the sulfur cathode and the dendrite-growth related battery failure arising from the use of a metallic lithium anode are addressed. Taking advantage of the highly soluble sulfur species, this work explores the possibility of using redox-active species with highly positive potential to couple with a sulfur anolyte for a redox flow battery. When paired with an aqueous bromide catholyte, a sulfur–bromine ($S–Br_2$) battery with the desired metal-free characteristic is successfully demonstrated. The battery exhibits a cell voltage exceeding 1.8 V, a specific capacity of $\sim$1600 mA h g^{-1}, coulombic efficiency approaching 100% and decent cycling efficiencies over 100 cycles. A full-liquid flow-through mode is able to be realized with a controlled depth of charge. Moreover, a high energy density can be expected with highly concentrated electrolytes, guaranteeing a promising sustainable energy storage technology candidate for both stationary and mobile applications.

1. Introduction

High-energy-density rechargeable batteries are of paramount interest and are under vigorous investigation because of the ubiquitous demand for energy storage devices in flourishing sustainable energy fields. It has long been known that under ambient conditions elemental sulfur (S_8) exists primarily in the form of an eight-membered ring, which provides a theoretical capacity of 1675 mA h g^{-1} through a multi-electron redox conversion involving multiphase transformation ($16Li + S_8 \leftrightarrow Li_2S$), far exceeding that of intercalation-type cathode materials.[1–3] Therefore, a fully packed lithium–sulfur (Li–S) battery promises up to two-fold specific energy improvement compared with the commercial lithium-ion battery.[3] Broad adoption of Li–S batteries, however, has been hampered by a series of obstacles. The major problems originate from sulfur chemistry related to the intrinsic electrical insulating features of sulfur, large volumetric change of sulfur species and shuttle effect of electrolyte–soluble intermediate products of lithium polysulfides (Li_2S_n, $4 \leq n \leq 8$).[3,4] During cycling, Li_2S_n may diffuse

throughout the cells, triggering parasitic reactions with the metallic Li anode and consequently leading to active material loss, serious corrosion reactions on the Li–metal surface and inhomogeneous aggregation of sulfur. Another issue involves the use of the Li anode. Significant challenges remain for its practical application such as dendrite formation and poor cycling efficiency.

Preventing the diffusion and non-electrochemical reactions of polysulfides is the key to tackling these obstacles. Extensive efforts have thus far been made to address this including impregnation of sulfur into various conductive matrixes,[5–8] employment of metal oxides[9–12] or metal sulfides[13–15] through chemical absorption of Li_2S_n, exploitation of alternative electrolytes to mitigate Li_2S_n solubility,[16–18] *etc.* As a matter of fact, when a liquid organic electrolyte is used, diffusion of continuously generated soluble polysulfide species is thermodynamically inevitable. Replacement of sulfur with Li_2S as a cathode should be a promising solution to address the concerns regarding the use of metallic lithium, because the fully lithiated Li_2S can be used as a Li source to potentially couple with Li-free materials.[19–22] Unfortunately, batteries with Li_2S cathodes suffer from some of the sulfur shortcomings (*e.g.*, low conductivity and dissolution). In addition, owing to the inherent instability of Li_2S in an ambient atmosphere, it is rather difficult and complex to handle Li_2S.

New approaches are emerging on how to overcome these issues. Taking advantage of the highly soluble sulfur species to develop semi-liquid Li–S batteries with liquid-phase sulfur-based cathodes is a plausible strategy.[23–25] A flow-through mode for the liquid electrode can be extended, which enables

[a] State Key Laboratory for Modification of Chemical Fibers and Polymer Materials, College of Materials Science and Engineering, Innovation Center for Textile Science and Technology, Donghua University, Shanghai 201620, China. E-mail: linawang@dhu.edu.cn; txliu@dhu.edu.cn

[b] Department of Chemistry, Shanghai Key Laboratory of Molecular Catalysis and Innovative Materials, Institute of New Energy, Collaborative Innovation Center of Chemistry for Energy Materials, Fudan University, Shanghai 200433, China. E-mail: yyxia@fudan.edu.cn

† Electronic supplementary information (ESI) available. See DOI: 10.1039/c8ta07951j

more flexible system customization. One of the advantages of flow batteries is the decoupling of power and energy, either by increasing the number of electrode pairs for higher power output, or by increasing the size of the tank and concentration of electrolytes to store more energy.[26] Therefore, redox flow batteries are particularly well-suited for large-scale energy storage applications. The all-vanadium redox flow battery has been the widest commercially deployed system among the various redox flow batteries that have been studied.[27–29] It exhibits high power capability but suffers from limited earth-abundance of vanadium, high material cost and low energy density, which significantly reduce its competitiveness. The large capacity, high solubility in combination with abundance in nature and environmental benignity of sulfur species open up broad prospects for the future design of grid-scale energy storage with superb energy density. In spite of the fact that significant progress has been made in semi-liquid Li–S batteries, the safety concerns regarding utilization of a metallic Li anode remain unresolved.

Breakthroughs in rechargeable battery technologies would not be realized with incremental improvements in existing technologies, but rather by the development of novel energy storage concepts incorporating new materials and chemical processes. To tackle the aforementioned challenges of Li–S batteries, here, we propose an original metal-free battery system that depends on the reversible conversion chemistry between sulfur and flexible redox-active species. Instead of using Li–metal anodes, aqueous cathodes (catholytes) containing highly soluble active materials are employed to pair with soluble sulfur-based anodes (anolytes). Generally, the game-changing shift requires a class of redox-active species with highly positive potential and low molecular weight to maximize the cell voltage and energy density. This restriction narrows the range of redox couples that could be selected. Among various redox couples (Fig. S1†),[26,30–35] the ones with high redox potential above 1 V (vs. SHE) but below the threshold of O_2 evolution by water electrolysis (1.23 V vs. SHE)[30,36] are within the scope of consideration. Among them, the highly soluble Br_3^-/Br^- couple is one of the most feasible candidate since its elemental abundance, acceptable specific capacity (331 mA h g^{-1} based on Br_2), and appropriate redox potential (ca. 1.05 vs. SHE, 4.1 V vs. Li/Li$^+$) are within the potential range of water electrolysis.[26,33–35] In the aqueous phase, bromide ions can combine with bromine molecules to generate tribromide ions ($Br^- + Br_2 \rightarrow Br_3^-$), significantly increasing their solubility; thus, relatively high concentrations of Br^- and Br_2 can be utilized.[26,33–35] Therefore, to achieve the desired full-liquid characteristic with high safety, high performance and high energy density, a sulfur–bromine (S–Br_2) battery using sulfur-based anolytes coupled with bromide-based catholytes is demonstrated as a model battery chemistry. In this initial proof-of-concept study, the most common electroactive species explored in the anolyte is elemental sulfur. A basic but systematic study in terms of electrochemical performance, reaction kinetics, and morphological transformations is discussed. The sufficient specific capacity, zero self-discharge, superior cycling stability and coulombic efficiency (CE) make the S–Br_2 battery a promising

sustainable energy storage technology candidate. Moreover, high energy density is able to be achieved with highly concentrated electrolyte solutions, offering new opportunities for designing next-generation rechargeable batteries.

2. Experimental section

2.1. Cell assembly

The cells were composed of two glass cylinders and a separator. For the assembly of S–Br_2 cells, a current collector of Super P carbon (Timcal)-loaded Ti foil (99.5%, 0.2 mm in thickness, Nilaco) was stuck on one open end of each glass cylinder. The geometric area of the cast carbon was 9 mm in diameter. The other open end of the glass cylinders was covered by a Li$^+$-conductive glass–ceramic membrane, $Li_{1+x+y}Al_xTi_{2-x}Si_yP_{3-y}O_{12}$ (LATP, 180 μm in thickness, 10^{-4} S cm^{-1} at 298 K, Ohara Corporation). The preparation and assembly of the anode side were conducted in an Ar-filled glovebox (<1 ppm of H_2O and O_2, Mikrouna). The anolyte solution was prepared by dissolution of 0.1 M sulfur (S) (99%, Wako Chemicals) and 1 M $LiClO_4$ (99.9%, Sigma Aldrich) into super-dehydrated tetrahydrofuran (THF, stabilizer free, ≥99.9%, Aladdin) in the glovebox. The transparent solution was added into one of the glass cylinders with a total volume of 150 μL. The aqueous catholyte solution containing 0.3 M LiBr (99.9%, Aladdin) and 1 M KBr (≥99.5%, Sigma Aldrich) was added into another glass cylinder with the same volume of 150 μL. For a control experiment, a anolyte solution with Li_2S_8 was prepared by mixing sulfur and Li_2S powders at a molar ratio of 7/1 for S/Li_2S in addition to 1 M $LiClO_4$ in the THF solvent. The resulting dark-brown solution contains 1/8 M Li_2S_8. The corresponding aqueous catholyte contains 3 M LiBr and 2 M KBr. The preparation and assembly of Li–LiBr and Li–S half cells were carried out in a manner similar to previous reports.[25,33] In brief, a lithium electrode was prepared by pressing a lithium metal sheet onto a copper mesh, which was welded onto a piece of copper foil. The Li metal sheet was immersed into an organic liquid electrolyte of 1 M $LiPF_6$ dissolved in ethylene carbonate (EC)/dimethyl carbonate (DMC)/diethyl carbonate (DEC) (1 : 1 : 1 by volume). A distance of about 1 mm was left between the Li metal and LATP to prevent the formation of a resistive precipitation-layer from the ceramic separator.[37]

2.2. Electrochemical measurements

If not specially mentioned, the electrochemical measurements were performed at 25 °C. Electrochemical impedance spectroscopy (EIS) and cyclic voltammetry (CV) were performed on a CH Instruments potentiostat (CHI660E). The frequency region for EIS was set to 10^6 to 0.1 Hz. CV curves were recorded in a potential window of 1.0–2.5 V for S–Br_2 cells and were not corrected for capacitance. The galvanostatic charge–discharge experiments were performed on a LAND CT2001A Battery Cycler (Wuhan, China) in a potential window of 1.5–3.0 V (vs. Li/Li$^+$) for Li–S half cells, 3.5–4.35 V (vs. Li/Li$^+$) for Li–LiBr half cells, and 1.0–2.5 V for S–Br_2 cells. The specific capacity is calculated based on the electroactive species of S or LiBr content. The

normalized capacity represents the fraction of capacity accessed compared to what is theoretically expected.

2.3. Characterization

Morphological information was obtained from scanning electron microscopy (SEM) using a scanning microscope (S-4800, HITACHI). Ultraviolet-visible absorption spectroscopy (UV-vis, UV-3600 spectrophotometer, Shimadzu) was used to examine the dissolved electrochemically active species in electrolytes. The contact angle was measured on a contact angle goniometer (OCA40Micro, Dataphysics).
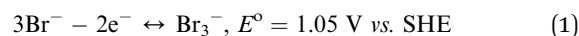
3. Results and discussion

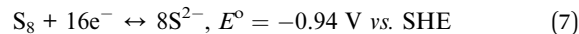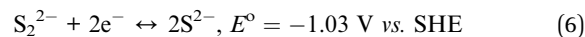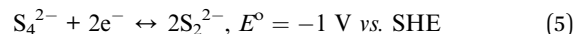### 3.1. Operating principle of the S–Br$_2$ rechargeable batteries
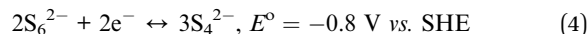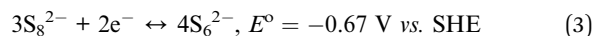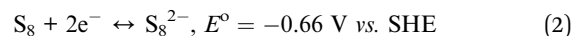
A schematic of the operating principle of this system is shown in Fig. 1a. A colorless KBr–LiBr aqueous solution was used as the catholyte. LiBr is able to serve as both the electrolyte component and also the active material. KBr is the supporting electrolyte used to stabilize the predictive products of Br$_2$ upon charging. To prevent the oxidation of Br$^-$ to BrO$^-$ as well as increase the threshold potential of the O$_2$ evolution reaction, the pH value of the catholyte was tuned to make it weakly acidic (Fig. S2†).[33] A colorless THF solution containing dissolved

Fig. 1 The design concept of a metal-free full-liquid S–Br$_2$ flow battery. (a) A schematic illustration of the proposed S–Br$_2$ flow battery. (b) Typical charge–discharge profiles of a Li–S half cell with a THF solution containing 0.1 M S and 1 M LiClO$_4$ and a Li–LiBr half cell with an aqueous solution in the presence of 0.3 M LiBr and 1 M KBr at a current density of 0.02 mA cm^{-2}.

elemental sulfur and LiClO$_4$ was used as the anolyte. The redox chemistry of the S–Br$_2$ battery is based on the Br$_3^-$/Br$^-$ couple in the catholyte and the S$_8$/8S^{2-} couple in the anolyte. The Br$_3^-$/Br$^-$ redox reaction ideally occurs at 1.05 V vs. SHE via a two-electron transfer as shown in eqn (1). The oxidation of Br$^-$ to Br$_3^-$ is often described in two steps via the formation of Br$_2$ firstly (2Br$^-$ − 2e$^-$ ↔ Br$_2$).[26,33–35] The free Br$_2$ is then stabilized by the Br$^-$ in the solution to form Br$_3^-$ (Br$_2$ + Br$^-$ → Br$_3^-$), i.e., the concentration of free Br$_2$ is low in the presence of excess Br$^-$. A multistage redox process may take place for the electrochemical reduction of sulfur as shown in eqn (2)–(6).[23,25] The overall reaction can be expressed as eqn (7) via 2 electrons per sulfur transfer with a calculated redox potential of −0.94 V vs. SHE. Thus, a theoretical equilibrium cell potential of 1.99 V can be expected for the proposed S–Br$_2$ cell (eqn (8)) according to the potential difference between Br$_3^-$/Br$^-$ and S$_8$/8S^{2-}. In brief, upon charging, Br$^-$ is oxidized to Br$_2$, followed by fast complexation with Br$^-$ to form more stable Br$_3^-$. Simultaneously, Li$^+$ migrates toward the anolyte across a Li$^+$ selective membrane while electrons travel through the external circuit to reach the surface of the negative electrode. Sulfur is thereby reduced by the incoming electrons to sulfide ions. The reaction directions are reversed during the discharge process. The operating principle of the present hybrid aqueous–non-aqueous S–Br$_2$ system is intrinsically different from that of the prior aqueous bromine–polysulfide system employing NaBr/Na$_2$S$_4$ electrolytes, wherein the redox chemistry is dependent on the redox reaction between Br$_3^-$/Br$^-$ and S$_4^{2-}$/2S$_2^{2-}$, giving rise to a working voltage of 1.36 V.[38–41]

Catholyte:

$$3Br^- - 2e^- \leftrightarrow Br_3^-, \quad E^\circ = 1.05 \text{ V } vs. \text{ SHE} \tag{1}$$

Anolyte:

$$S_8 + 2e^- \leftrightarrow S_8^{2-}, \quad E^\circ = -0.66 \text{ V } vs. \text{ SHE} \tag{2}$$

$$3S_8^{2-} + 2e^- \leftrightarrow 4S_6^{2-}, \quad E^\circ = -0.67 \text{ V } vs. \text{ SHE} \tag{3}$$

$$2S_6^{2-} + 2e^- \leftrightarrow 3S_4^{2-}, \quad E^\circ = -0.8 \text{ V } vs. \text{ SHE} \tag{4}$$

$$S_4^{2-} + 2e^- \leftrightarrow 2S_2^{2-}, \quad E^\circ = -1 \text{ V } vs. \text{ SHE} \tag{5}$$

$$S_2^{2-} + 2e^- \leftrightarrow 2S^{2-}, \quad E^\circ = -1.03 \text{ V } vs. \text{ SHE} \tag{6}$$

$$S_8 + 16e^- \leftrightarrow 8S^{2-}, \quad E^\circ = -0.94 \text{ V } vs. \text{ SHE} \tag{7}$$

Overall cell reaction:

$$24Br^- + S_8 \leftrightarrow 8Br_3^- + 8S^{2-}, \quad E^\circ_{cell} = 1.99 \text{ V} \tag{8}$$
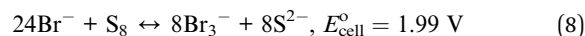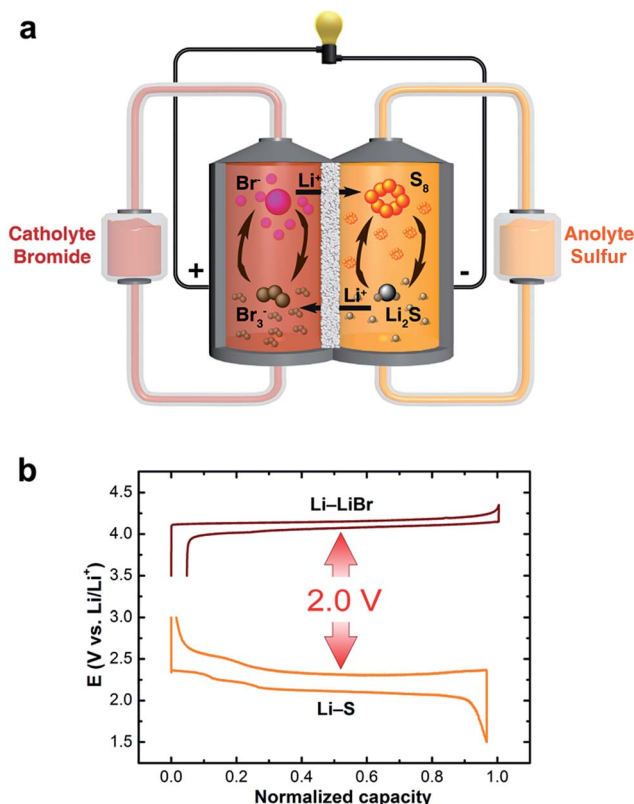
The electrochemical activity of the catholyte and anolyte was firstly explored in half cells with a Li–metal counter/reference electrode (Fig. 1b). The galvanostatic charge–discharge profiles of Li–LiBr half cells, recorded from 3.5 to 4.35 V (vs. Li/Li$^+$), show one pair of flat charge/discharge plateaus at 4.16 and 4.08 V respectively, corresponding to the electrochemical oxidation of Br$^-$ and reduction of Br$_3^-$. Multistep reactions are

This journal is © The Royal Society of Chemistry 2018

J. Mater. Chem. A, 2018, **6**, 20737–20745 | 20739

indicated by the charge–discharge profiles of Li–S half cells, of which three sequential discharge voltage plateaus at 2.34, 2.24 and 2.10 V and reversible charge plateaus can be observed. Both of the Li–LiBr and Li–S half cells demonstrate a stable voltage plateau, ≥97% utilization of active materials and ≥95% CE. Such electrochemical characteristics are desired for smooth operation of a S–Br$_2$ full cell.

3.2. Rechargeability of the S–Br$_2$ batteries

To verify the reversibility of the proposed S–Br$_2$ battery, the electrochemical behavior was firstly evaluated *via* CV. The capacity ratio of anolyte (THF solution containing 0.1 M S and 1 M LiClO$_4$) to catholyte (aqueous solution containing 0.3 M LiBr and 1 M KBr) is 0.7 : 1 with the same volume, *i.e.*, sulfur is the capacity-limiting-side. The open-circuit potential (OCP) of an as-assembled fresh S–Br$_2$ cell is ~0.6 V. The S–Br$_2$ cell was initially swept from OCP to 2.5 V and then from 2.5 to 1 V. A representative CV curve in Fig. 2a shows three apparent successive cathodic current peaks at 1.66 (I_{c1}), 1.84 (I_{c2}) and 2.09 V (I_{c3}), suggesting a stepwise reduction process from elemental sulfur to sulfides. The initial reduction step is likely associated with opening of the ring-shaped S$_8$ and the subsequent processes lead to breakage of linear polysulfide chains towards the lower order. A broad anodic peak (I_a) centered at 1.56 V appears with an obvious shoulder peak at 1.45 V, suggesting that the oxidation reactions allow for reconnection of chains from sulfides to polysulfides and elemental sulfur upon

the reverse sweep from 2.5 to 1.0 V. A larger potential difference between the reduction and oxidation peaks is exhibited at higher sweep rates (Fig. 2b). The reaction kinetics can be analyzed according to the relationship between the measured current (I) and the scan rate (v) from the CV curves: $I = av^b$, where a and b are adjustable parameters.[42] The current response to an applied sweep rate will vary depending on whether the redox reaction is diffusion-controlled or surface-controlled. The well-defined condition is $b = 0.5$ for a redox reaction limited by a semi-infinite linear diffusion, whereas the current varies with v directly for a capacitive process.[43] Since the plot of I *vs.* $v^{-1/2}$ is not entirely linear diffusion (Fig. S3†), the value of b is determined from the slope of the log I *vs.* log v plot (Fig. 2c). Except for the b-value of I_{c2}, which is 0.82, the other peak currents show a b-value approaching 0.5. The results indicate that the redox reactions in the S–Br$_2$ system are approximately diffusion-controlled. Probably, the metastable and quick reaction process at I_{c2} induces the surface-controlled contribution.

Further galvanostatic charge–discharge testing demonstrates steady-state voltage plateaus, high utilization ratio of active materials and remarkable rechargeability of the S–Br$_2$ battery. Fig. 2d presents the typical charge–discharge curves of the as-prepared S–Br$_2$ cell when continuously operated at 0.02 mA cm^{-2} in the voltage range from 1 to 2.5 V. The specific capacity during the 1st charge reaches 1645 mA h g^{-1}, 98% of the theoretical capacity of sulfur. However, the reversible
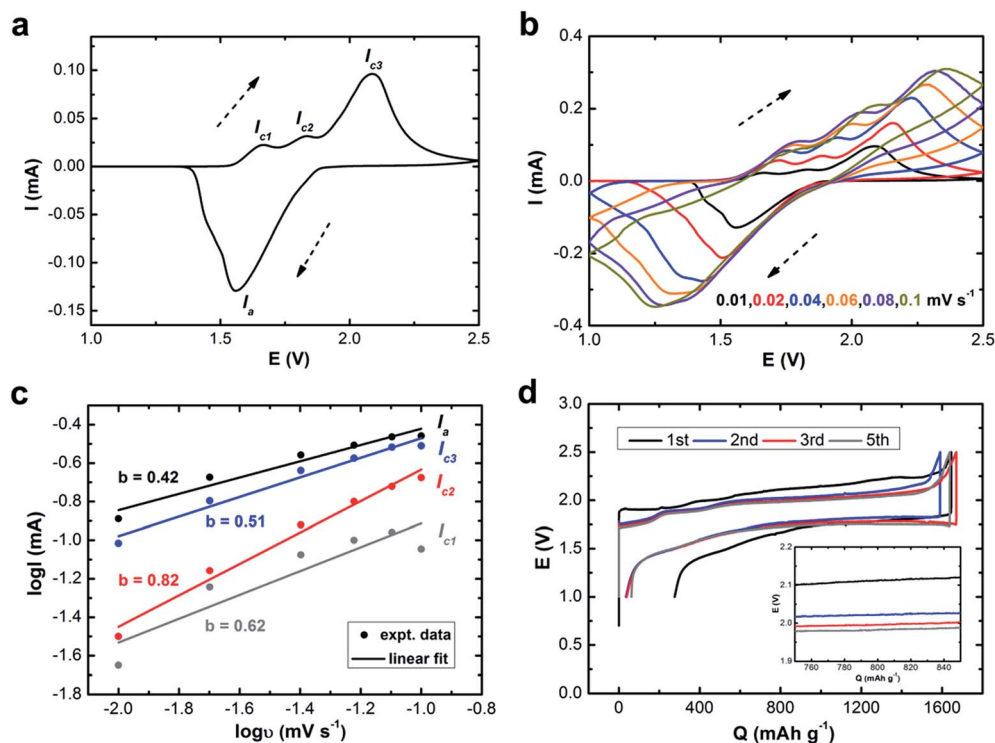

Fig. 2 Rechargeability of the S–Br$_2$ battery. (a) CV curve at a sweep rate of 0.01 mV s^{-1}. (b) CV curves at various sweep rates. (c) Relationship between the logarithm of peak currents (log I) and the logarithm of sweep rates (log v). (d) Galvanostatic charge–discharge profiles for 5 cycles at a current density of 0.02 mA cm^{-2}. The inset is the enlargement of the charge profiles in the range of 750–850 mA h g^{-1}. The anolyte is a THF solution containing 0.1 M S and 1 M LiClO$_4$. The catholyte is an aqueous solution in the presence of 0.3 M LiBr and 1 M KBr.

20740 | *J. Mater. Chem. A*, 2018, **6**, 20737–20745

This journal is © The Royal Society of Chemistry 2018

specific capacity during the 1st discharge is only 1369 mA h g^{-1}, indicating an initial CE of 83%. In the consecutive cycles, the reversible capacity is significantly enlarged and approaches 1632 mA h g^{-1} with a 98% CE in the 3rd cycle. A high reversible capacity is retained in the subsequent cycles. In accordance with the CV in Fig. 2a and b, the voltage curves of the S–Br$_2$ cell clearly show three voltage plateaus upon charge and discharge processes. Taking the 3rd charge profile for instance, the first voltage plateau at 1.76 V displays a specific capacity of approximately 209 mA h g^{-1}, accounting for 12.5% of the total charge capacity. The value is in accordance with the theoretical specific capacity of the reduction reaction from S$_8$ to Li$_2$S$_8$ (209 mA h g^{-1}, 209/1675 = 12.5%). The consecutive second plateau at 1.89 V displays a specific capacity of 220 mA h g^{-1}, suggesting the conversion reaction from Li$_2$S$_8$ to Li$_2$S$_4$, while the last long voltage plateau at 2.0 V accounts for ~74% of the total charge capacity, indicating the predominant reduction process of Li$_2$S$_4$ → Li$_2$S. The theoretical specific capacity of the reduction from Li$_2$S$_4$ to Li$_2$S is 1256 mA h g^{-1}, corresponding to 75% of theoretical capacity of sulfur (1256/1675 = 75%).

The apparently efficient reversibility between Br$_3^-$/Br$^-$ and S$_8$/8S^{2-} is revealed for the first time to the best of our knowledge. It is noteworthy that there is obvious overpotential during the 1st charge. An approximately 90 mV potential difference is presented between the 1st and 2nd charge profiles at the point of 800 mA h g^{-1} (inset of Fig. 2d). The overpotential during the 5th charge is decreased by 130 mV compared with the 1st charge. A similar remarkable potential difference during the initial cycles appears for Li–LiBr half cells (Fig. S4a†),[33] but not for Li–S half cells (Fig. S4b†). Such polarization is expected due to the large interfacial charge transfer resistance between the aqueous LiBr–KBr catholyte and the hydrophobic conductive carbon-coated current collector. For clarification, the hydrophilicity of the carbon film surface was tested with a contact angle goniometer. In comparison with the pristine current collector, the contact angle is reduced from 144 to 131.3° after the 1st cycle (Fig. S5a and b†), implying that the carbon surface becomes less hydrophobic with the catholyte. In the following cycles, from the 2nd to the 5th cycle, the contact angle changes slightly from 131.3 to 128.6° (Fig. S5c†), in accordance with the small overpotential drop over repeated cycling. In contrast, the sulfur-based anolyte shows excellent wettability with the carbon surface (Fig. S5d†). The improved wetting means that a higher surface area of the carbon electrode is in intimate contact with the electrolyte, thereby providing increased surface area and reduced interfacial charge transfer resistance, reflected by the diminished polarization upon cycling. In addition, the EIS analysis provides compelling evidence of the dramatically decreased interfacial resistance of both S–Br$_2$ and Li–LiBr cells after the initial cycle (Fig. S6a and b†).

However, the comparatively low CE of 83% in the 1st cycle of the S–Br$_2$ cell should not simply be due to the hydrophobic carbon surface. At the same current density, a higher initial CE of 92% can be reached for the Li–LiBr half cell (Fig. S4a†), while the Li–S half cell displays 86% initial CE (Fig. S4b†). With increased current densities of 0.03, 0.05 and 0.1 mA cm^{-2}, the S–Br$_2$ cells present even lower initial CE of 82, 76 and 67%,

respectively (Fig. S7†). To gain deep insight into the redox reactions in S–Br$_2$ cells, UV-vis absorption spectra of the catholyte and anolyte at their pristine, fully charged and fully discharged states were tested. After the 1st charge, the identification of the characteristic absorption peak at 266 nm evidences the generation of Br$_3^-$ (Fig. 3a).[35] Also we observed that the colorless catholyte turned into a transparent yellowish solution during charging. After the 1st discharge, the UV-vis signals representing Br$_3^-$ (inset of Fig. 3a) reveal that Br$_3^-$ would not be completely reduced to Br$^-$. For the pristine anolyte, the strong absorption of elemental sulfur is detected at around 220 and 270 nm (Fig. 3b).[44] A small absorption peak at 209 nm likely associated with S$_n^{2-}$ appears after the 1st charge, indicating that the elemental sulfur might not be fully converted to Li$_2$S. The precipitation and dissolution behavior of Li$_2$S from the anolyte solution is another important parameter for understanding the S–Br$_2$ chemistry, which was investigated by SEM of the carbon current collector (Fig. S8†). SEM images reveal that the Li$_2$S precipitation is formed during the 1st charge. However, residual particles are observed after the 1st discharge, revealing that Li$_2$S is not fully decomposed. No precipitation is observed on the carbon film at the catholyte side. These results suggest that the slow conversion of solid and insulated Li$_2$S deposits to soluble polysulfides contributes much to the initial 17% irreversibility. Interestingly, the specific capacity of the 2nd charge, 1590 mA h g^{-1}, is obviously higher than the specific capacity of the 1st discharge, 1369 mA h g^{-1}. The result indicates that some of the residual Li$_2$S particles are activated upon subsequent cycling. Indeed, it can be assumed that the operation of the sulfur anolyte involves both electrochemical and chemical reactions. As discussed in our previous work with a Li$_2$S cathode,[21] the liquid charge/discharge intermediate products (e.g., long-chain polysulfides) can oxidize the solid Li$_2$S through direct chemical reactions. The products of polysulfides from such chemical reactions can be further electrochemically reduced/oxidized in the subsequent charge–discharge process. Therefore, both the electrochemical and chemical reactions prompt the delithiation of Li$_2$S (as illustrated in Fig. S9†). The reaction kinetics is increased through activation and stabilization of electrochemically active species, resulting in a significantly enlarged reversible capacity and almost 100% CE. After repeated cycling, no obvious Li$_2$S particles can be observed by SEM. The regeneration of S$_8$ absorption peaks and the weak Br$_3^-$ UV-vis signals strongly support the stable redox chemistry of the S–Br$_2$ battery.

3.3. Further electrochemical characteristics of the S–Br$_2$ rechargeable batteries

Fig. 4a and b show profiles of the S–Br$_2$ battery for 30 cycles at a current density of 0.05 mA cm^{-2}. The capacity is activated to approximately 1100 mA h g^{-1} during the initial 5 cycles and is then retained in the subsequent cycles without significant capacity fading. At an even higher current density of 0.1 mA cm^{-2} (Fig. 4c and d), the steady-state charge–discharge curves reveal that a reversible capacity of 831 mA h g^{-1} is delivered until the 20th cycle. And a capacity retention of 98%

This journal is © The Royal Society of Chemistry 2018

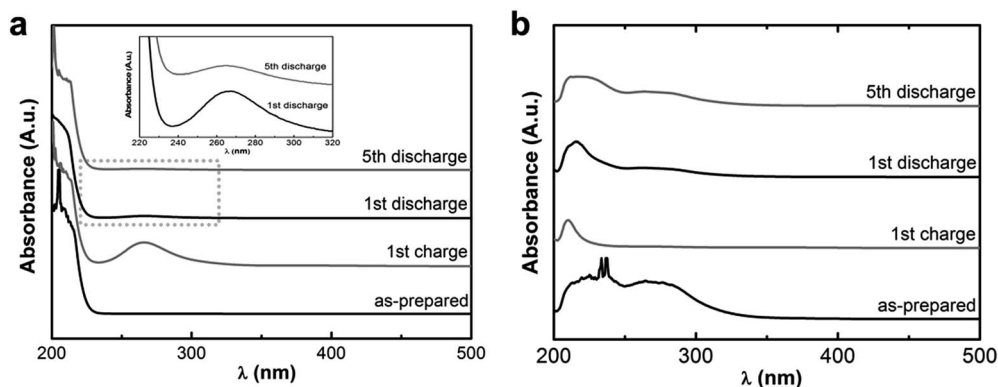*J. Mater. Chem. A*, 2018, **6**, 20737–20745 | **20741**

Fig. 3 UV-vis spectra of (a) catholytes and (b) anolytes. The inset in (a) is the enlargement of the dashed box in the range of 220–320 nm. The as-prepared samples were examined after the 1st charge, after the 1st discharge and after the 5th discharge.

(810 mA h g⁻¹) is achieved after 100 cycles. Considering the high or moderate ionic conductivity of Li⁺ in the aqueous phase ($\sim10^{-2}$ S cm⁻¹) or organic electrolyte ($\sim10^{-3}$ S cm⁻¹),[33,36,45] the slower polysulfide activation and decreased capacity at increased current densities should be ascribed to the slow mobility of Li⁺ in the Li⁺ ceramic membrane (10^{-4} S cm⁻¹ at room temperature).[31] Development of a suitable lithium superionic conductor with a higher ionic conductivity, however, is still ongoing. Otherwise, this limitation can be mitigated by elevating the temperature, which logarithmically enhances the conductivity of the Li⁺ ceramic membrane, as evidenced by a higher reversible capacity of approximately 1600 mA h g⁻¹ at 0.05 mA cm⁻² when operated at 30 °C (Fig. 5a). At 0.1 mA cm⁻²,

a reversible capacity above 1300 mA h g⁻¹ is able to be delivered (Fig. S10†).

The rate performance of the S–Br₂ battery indicates that 98%, 85%, 73%, 60%, 48%, 39%, 21% and 10% of the theoretical specific capacity could be retained at 0.05, 0.1, 0.15, 0.2, 0.25, 0.3, 0.4 and 0.5 mA cm⁻² at 30 °C (Fig. 5b). As the current density further increases, both potential drop and capacity loss become more obvious. The power density of the S–Br₂ battery is estimated from the polarization curve (Fig. S11†); a power density of 0.64 mW cm⁻² is obtained with a corresponding current density of 0.5 mA cm⁻² and a midpoint discharge voltage of 1.28 V. A maximum power density approaching 0.8 mW cm⁻² can be expected from the parabolic evolutional
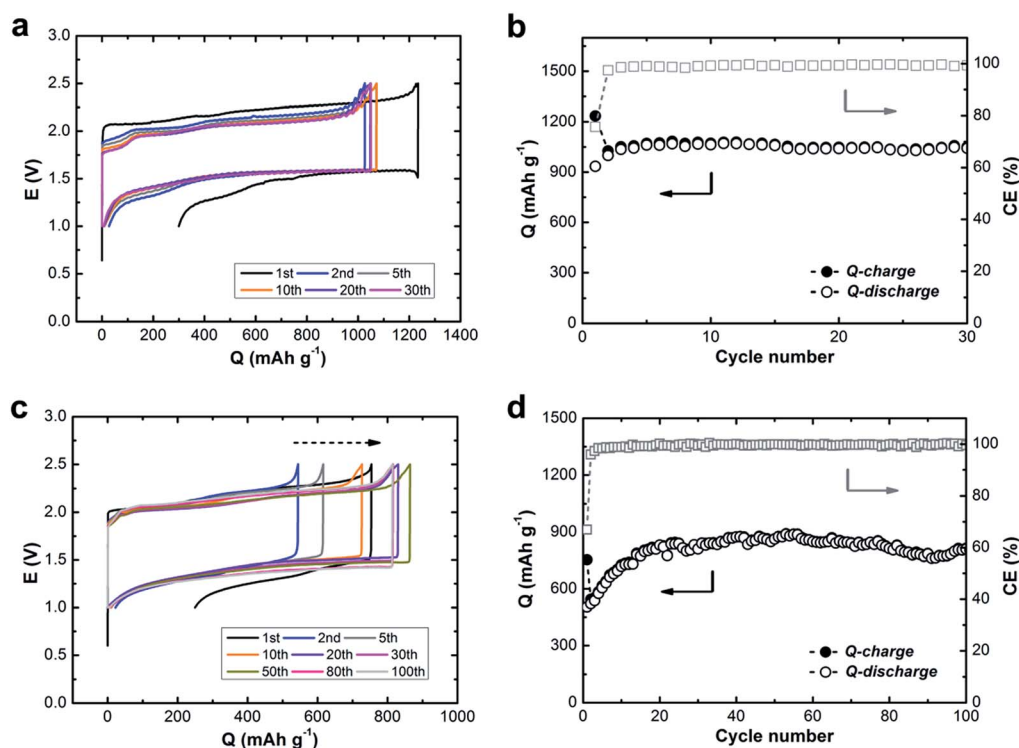

Fig. 4 Cycling performance of the S–Br₂ batteries. (a and c) Galvanostatic charge–discharge profiles for repeated cycling at (a) 0.05 mA cm⁻² and (c) 0.1 mA cm⁻². (b and d) The corresponding cycling performance with respect to specific capacity (Q) and coulombic efficiency (CE).
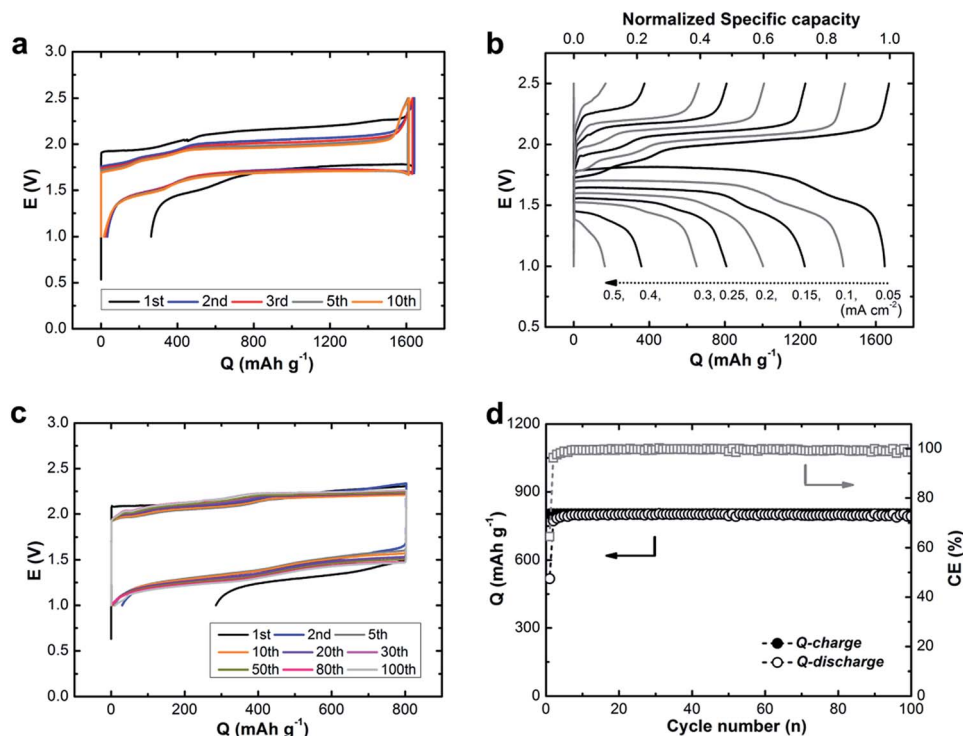
20742 | *J. Mater. Chem. A*, 2018, **6**, 20737–20745

This journal is © The Royal Society of Chemistry 2018

Fig. 5 Electrochemical performance of the S–Br$_2$ batteries at an increased temperature of 30 °C. (a) Galvanostatic charge–discharge profiles for 10 cycles at 0.05 mA cm^{-2}. (b) Rate capability at various current densities. (c) Galvanostatic charge–discharge profiles measured by controlling the charge specific capacity to 800 mA h g^{-1} and cut-off voltage to 1.0 V at 0.1 mA cm^{-2}. (d) The corresponding cycling performance with respect to Q and CE.

tendency with increased current density. The linear polarization curve indicates that the performance of the battery is dominated by its resistance. During the charge–discharge processes, the electroactive sulfur in the anolyte exhibits a phase change $(S_8 \text{ (liquid)} \leftrightarrow S_n^{2-} \text{ (liquid)} \leftrightarrow Li_2S \text{ (solid)})$ while the bromide does not $(Br^- \text{ (liquid)} \leftrightarrow Br_3^- \text{ (liquid)})$, implying that the power and energy density might not be so fully decoupled as in a flow battery in practice. For the potential extension to an efficient full-liquid flow-through mode, wherein the soluble catholyte and the anolyte can be stored in external reservoirs and circulated with the assistance of an external circulating sub-system, the mass precipitation of Li$_2$S can be avoided by the shrinkage of the cut-off voltage window. Fig. 5c and d demonstrate the short term cycling performance measured by controlling the charge specific capacity to 800 mA h g^{-1} and cut-off voltage to 1.0 V. No capacity decay is observed over 100 cycles with a 100% CE, confirming the reversible and effective electrochemical energy conversion between sulfur and bromine. Low self-discharge is another important criterion to judge the practicality of an energy-storage device. For conventional Li–S batteries, self-discharge always occurs when the batteries are resting due to the internal polysulfide shuttle effect.[46] Soluble long-chain polysulfide species would continue to be dissolved and migrate to the negative side to react with metallic Li. This issue can be addressed with the introduced S–Br$_2$ system by preventing polysulfide anions from passing through the separator to avoid the unwanted side reactions, as confirmed by the suppressed self-discharge behavior (Fig. S12†). When the cell is

rested for one day after charge to 2.5 V, the open-circuit cell voltage remains stable at 1.91 V in the fully charged state. There is no detection of self-discharge with almost 100% charge–discharge efficiency.

Elemental sulfur exhibits limited solubility in the vast majority of organic solvents. The maximum solubility of sulfur in THF is about 0.3 M (on the basis of S) at room temperature. To achieve higher volumetric energy density, highly concentrated electrolyte solutions need to be used. Long-ordered polysulfides generally have a higher solubility compared to elemental sulfur. Hence, we prepared highly concentrated 1/8 M Li$_2$S$_8$, *i.e.*, 1 M S by mixing sulfur and Li$_2$S powders in a 7 : 1 ratio (7S + Li$_2$S → Li$_2$S$_8$). The anolyte solution displays a dark-brown color, implying the presence of highly concentrated polysulfides. At room temperature (25 °C), the S–Br$_2$ cell delivers a stable capacity of more than 700 mA h g^{-1} with a CE of 98% at 0.05 mA cm^{-2} (Fig. S13†). The lower specific capacity compared to that obtained with a fivefold lower concentration of active material in Fig. 4a is attributed to the accumulation of a thick Li$_2$S layer and the sluggish mass transport of polysulfides in the highly concentrated solution. At an increased temperature of 30 °C, the volumetric capacity reaches 11 A h L^{-1} at 0.1 mA cm^{-2} based on the total volume of the catholyte and anolyte (Fig. 6), indicating a volumetric energy density of around 20 W h L^{-1}. And the volumetric capacity could be held at around 8.5 A h L^{-1} at an increased current density of 0.5 mA cm^{-2}. A higher energy density can be expected given that the saturated concentration of S (in the form of Li$_2$S$_n$) in organic solutions is as high as 10 M.[47]
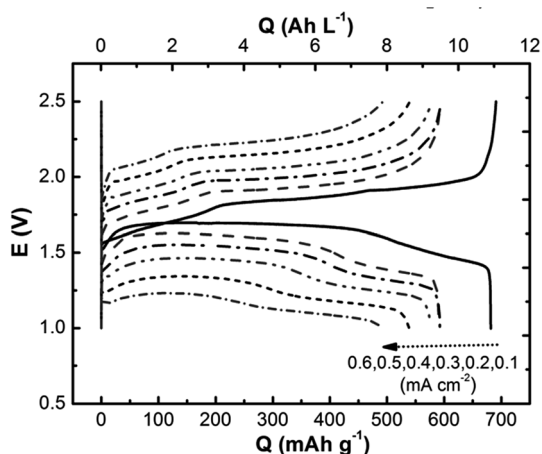
Fig. 6 Galvanostatic charge–discharge profiles of the S–Br$_2$ battery with a high concentration of polysulfides at various current densities. The anolyte is a THF solution in the presence of 1/8 M Li$_2$S$_8$ and 1 M LiClO$_4$. The aqueous catholyte solution contains 3 M LiBr and 2 M KBr. The operation temperature is 30 °C.

The above results have demonstrated the efficient electrochemical energy conversion between sulfur and bromine, providing multiple potential possibilities for overcoming those problems in practical Li–S technology as well as guaranteeing a promising model for future redox flow systems with efficient utilization of sulfur. Firstly, the dendrite-growth related battery failure and safety hazards have been mitigated without using Li–metal electrodes. Besides the potential for internal short circuits, the short cycling life of metallic Li is another barrier to the development of Li–metal batteries. The low CE has to be partially compensated by using an excess amount of Li of at least 300%.[48] Secondly, unlike solid sulfur electrodes, which suffer from severe volume expansion/shrinkage during lithiation/delithiation, leading to deterioration of batteries, the redox reactions did not cause a volume change of electrodes in the proposed S–Br$_2$ system. The liquid electrolyte effectively buffers the phase changes of sulfur species, therefore achieving superior reversibility. Thirdly, the new cell design can be extended to a full-liquid flow-through mode. Therefore, the energy capacity can be independently scaled up, promising to be applicable to both the electric-vehicle market and electrical energy storage grids.

4. Conclusions

In conclusion, redox couples with highly positive potential can be applied in a metal-free full-liquid rechargeable battery based on a soluble sulfur anolyte for efficient electrical energy storage. Selection of redox-active species for aqueous catholytes is crucial to the development of the proposed system. In this study, a S–Br$_2$ battery is successfully demonstrated according to the potential difference between Br$_3^-$/Br$^-$ and S$_8$/8S^{2-}. It avoids using the potentially dangerous Li–metal and also a variety of heavy metals. The chemical species employed are abundant, their cost is reasonable and they are very soluble in liquid media. The cell operates without a catalyst and is efficiently rechargeable. The possibility of a full-liquid flow-through mode allows flexibility of the cell design. In spite of the fact that the slow mobility of Li$^+$ in the Li$^+$ ceramic membrane degrades the performance of the S–Br$_2$ system, a decrease in the resistance would dramatically improve the battery performance.

Conflicts of interest

There are no conflicts to declare.

Acknowledgements

Notes and references

1 M. S. Whittingham, *Chem. Rev.*, 2004, **104**, 4271–4302.
2 N.-S. Choi, Z. Chen, S. A. Freunberger, X. Ji, Y.-K. Sun, K. Amine, G. Yushin, L. F. Nazar, J. Cho and P. G. Bruce, *Angew. Chem., Int. Ed.*, 2012, **51**(40), 9994–10024.
3 P. G. Bruce, S. A. Freunberger, L. J. Hardwick and J. M. Tarascon, *Nat. Mater.*, 2012, **11**, 19–29.
4 A. Manthiram, Y. Fu and Y.-S. Su, *Acc. Chem. Res.*, 2013, **46**(5), 1125–1134.
5 J. Zhang, C.-P. Yang, Y.-X. Yin, L.-J. Wan and Y.-G. Guo, *Adv. Mater.*, 2016, **28**, 9539–9544.
6 L. Wang, Y. Zhao, M. L. Thomas and H. R. Byon, *Adv. Funct. Mater.*, 2014, **24**, 2248–2252.
7 W. Zhou, Y. Yu, H. Chen, F. J. Disalvo and H. D. Abruña, *J. Am. Chem. Soc.*, 2013, **135**(44), 16736–16743.
8 Z. Sun, M. Xiao, S. Wang, D. Han, S. Song, G. Chen and Y. Meng, *J. Mater. Chem. A*, 2014, **2**, 15938–15944.
9 H. Wang, T. Zhou, D. Li, H. Gao, G. Gao, A. Du, H. Liu and Z. Guo, *ACS Appl. Mater. Interfaces*, 2017, **9**(5), 4320–4325.
10 Y. Li, D. Ye, W. Liu, B. Shi, R. Guo, H. Zhao, H. Pei, J. Xu and J. Xie, *ACS Appl. Mater. Interfaces*, 2016, **8**, 28566–28573.
11 H. Yao, G. Zheng, P.-C. Hsu, D. Kong, J. J. Cha, W. Li, Z. W. Seh, M. T. McDowell, K. Yan, Z. Liang, V. K. Narasimhan and Y. Cui, *Nat. Commun.*, 2014, **5**, 3943.
12 X. Liu, J.-Q. Huang, Q. Zhang and L. Mai, *Adv. Mater.*, 2017, **29**(20), 1601759.
13 Q. Pang, D. Kundu and L. F. Nazar, *Mater. Horiz.*, 2016, **3**(2), 130–136.
14 Z. Yuan, H.-J. Peng, T.-Z. Hou, J.-Q. Huang, C.-M. Chen, D.-W. Wang, X.-B. Cheng, F. Wei and Q. Zhang, *Nano Lett.*, 2016, **16**(1), 519–527.
15 W. Wang, P. Yang, Z. Jian, H. Li, Y. Xing and S. Zhang, *J. Mater. Chem. A*, 2018, **6**, 13797–13805.
16 S. Chen, F. Dai, M. L. Gordin, Z. Yu, Y. Gao, J. Song and D. Wang, *Angew. Chem., Int. Ed.*, 2016, **55**(13), 4231–4235.
17 L. Wang, J. Liu, S. Yuan, Y. Wang and Y. Xia, *Energy Environ. Sci.*, 2016, **9**, 224–231.

20744 | *J. Mater. Chem. A*, 2018, **6**, 20737–20745

This journal is © The Royal Society of Chemistry 2018

18 S. Chen, Z. Yu, M. L. Gordin, R. Yi, J. Song and D. Wang, *ACS Appl. Mater. Interfaces*, 2017, **9**(8), 6959–6966.

19 Y. Yang, G. Zheng, S. Misra, J. Nelson, M. F. Toney and Y. Cui, *J. Am. Chem. Soc.*, 2012, **134**, 15387–15394.

20 S. Liang, Y. Xia, C. Liang, Y. Gan, H. Huang, J. Zhang, X. Tao, W. Sun, W. Han and W. Zhang, *J. Mater. Chem. A*, 2018, **6**, 9906–9914.

21 L. Wang, Y. Wang and Y. Xia, *Energy Environ. Sci.*, 2015, **8**, 1551–1558.

22 G. Tan, R. Xu, Z. Xing, Y. Yuan, J. Lu, J. Wen, C. Liu, L. Ma, C. Zhan, Q. Liu, T. Wu, Z. Jian, R. Shahbazian-Yassar, Y. Ren, D. J. Miller, L. A. Curtiss, X. Ji and K. Amine, *Nat. Energy*, 2017, **2**, 17090.

23 Y. Yang, G. Zheng and Y. Cui, *Energy Environ. Sci.*, 2013, **6**, 1552–1558.

24 N. Li, Z. Weng, Y. Wang, F. Li, H.-M. Cheng and H. Zhou, *Energy Environ. Sci.*, 2014, **7**, 3307–3312.

25 L. Wang, Y. Zhao, M. L. Thomas, A. Dutta and H. R. Byon, *ChemElectroChem*, 2016, **3**, 152–157.

26 Y. Zhao, Y. Ding, Y. Li, L. Peng, H. R. Byon, J. B. Goodenough and G. Yu, *Chem. Soc. Rev.*, 2015, **44**, 7968–7996.

27 W. Wang, S. Kim, B. Chen, Z. Nie, J. Zhang, G.-G. Xia, L. Li and Z. Yang, *Energy Environ. Sci.*, 2011, **4**, 4068–4073.

28 M. Skyllas-Kazacos, *J. Power Sources*, 2003, **124**, 299–302.

29 Z. Li, G. Weng, Q. Zou, G. Cong and Y.-C. Lu, *Nano Energy*, 2016, **30**, 283–292.

30 Y. Lu, J. B. Goodenough and Y. Kim, *J. Am. Chem. Soc.*, 2011, **133**, 5756–5759.

31 Y. Zhao, L. Wang and H. R. Byon, *Nat. Commun.*, 2013, **4**, 1896.

32 Y. Wang, Y. Wang and H. Zhou, *ChemSusChem*, 2011, **4**, 1087–1090.

33 Y. Zhao, Y. Ding, J. Song, J. B. Goodenough and G. Yu, *Energy Environ. Sci.*, 2014, **7**, 1990–1995.

34 K. Takemoto and H. Yamada, *J. Power Sources*, 2015, **281**, 334–340.

35 Z. Chang, X. Wang, Y. Yang, J. Gao, M. Li, L. Liu and Y. Wu, *J. Mater. Chem. A*, 2014, **2**, 19444–19450.

36 D. R. Lide, *CRC Handbook of Chemistry and Physics*, CRC Press, LLC, Boca Raton, FL, 3rd edn, 2000.

37 T. Zhang, N. Imanishi, S. Hasegawa, A. Hirano, J. Xie, Y. Takeda, O. Yamamoto and N. Sammes, *J. Electrochem. Soc.*, 2008, **155**, A965–A969.

38 A. Price, S. Bartley, S. Male and G. Cooley, *Power Eng. J.*, 1999, **13**(3), 122–129.

39 P. Morrissey, *Int. J. Ambient Energy*, 2000, **21**(4), 213–220.

40 F. C. Walsh, *Pure Appl. Chem.*, 2001, **73**(12), 1819–1837.

41 H. T. Zhou, H. M. Zhang, P. Zhao and B. L. Yi, *Electrochim. Acta*, 2006, **51**, 6304–6312.

42 H. Lindstrom, S. Sodergren, A. Solbrand, H. Rensmo, J. Hjelm, A. Hagfeldt and S. E. Lindquist, *J. Phys. Chem. B*, 1997, **101**, 7717–7722.

43 V. Augustyn, P. Simonbc and B. Dunn, *Energy Environ. Sci.*, 2014, **7**, 1597–1614.

44 C. Barchasz, F. Molton, C. Duboc, J.-C. Leprêtre, S. Patoux and F. Alloin, *Anal. Chem.*, 2012, **84**, 3973–3980.

45 K. Xu, *Chem. Rev.*, 2004, **104**, 4303–4417.

46 Y. V. Mikhaylik and J. R. Akridge, *J. Electrochem. Soc.*, 2004, **151**, A1969–A1976.

47 R. D. Rauh, K. M. Abraham, G. F. Pearson, J. K. Surprenant and S. B. Brummer, *J. Electrochem. Soc.*, 1979, **126**(4), 523–527.

48 W. Xu, J. Wang, F. Ding, X. Chen, E. Nasybulin, Y. Zhang and J.-G. Zhang, *Energy Environ. Sci.*, 2014, **7**, 513–537.

This journal is © The Royal Society of Chemistry 2018

J. Mater. Chem. A, 2018, **6**, 20737–20745 | **20745**